



Team Name: DJS SKYLARK - REGULAR CLASS

Team Number: 024

School Name: Dwarkadas J Sanghvi College of Engineering

TEAM MEMBERS

Team Captain: Fenil Vanani

Harmin Naik

Glenn Castellino

Chaitrali Chaudhari

Muskaan Mehta

Rushabh Gala

Ved Vartak

Dhairya Foria

Sharva Potdar

Shome Vakharia

Nainika Shah

Kirtan Jhaveri

Durvesh Deokar

Gaurang Raje

Heta Shah

Sucheta Kabra

Rishi Dasgupta

Jainam Gala

Aayush Shah

Siddharth Singh

Rishi Ghia

Raj Anadkat

Roshan Sam

Hiral Shah

Riyanshi Shah

Nishita Mehta

Shantanu Thorat

Jinay Gandhi

STATEMENT OF COMPLIANCE

Certification of Qualification

Team Name DJS Skylark – Regular Class Team Number 024
School Dwarkadas J. Sanghvi College of Engineering
Faculty Advisor Prof. Shashikant Auti
Faculty Advisor's Email shashikant.auti@gmail.com

Statement of Compliance

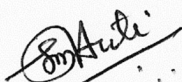
As faculty Adviser:

SA (Initial) I certify that the registered team members are enrolled in collegiate courses.

SA (Initial) I certify that this team has designed and constructed the radio controlled aircraft in the past nine (9) months with the intention to use this radio controlled aircraft in the 2020 SAE Aero Design competition, without direct assistance from professional engineers, R/C model experts; and/or related professionals.

SA (Initial) I certify that this year's Design Report has original content written by members of this year's team.

SA (Initial) I certify that all reused content has been properly referenced and is in compliance with the University's plagiarism and reuse policies.



Signature of Faculty Advisor



Signature of Team Captain



Table of Contents

List of Figures, Tables, Symbols, and Abbreviations	1
1.0 Executive Summary	2
1.1 System Overview and Discriminators	2
1.2 Competition Projections	3
2.0 Project Management	3
2.1 Schedule Summary	3
2.2 Personnel Management	4
2.3 Cost Report	4
3.0 Design Layout and Trades	5
3.1 Overall Design Features and Details	5
3.2 Competitive Scoring and Strategy	7
3.3 Design Derivation	8
3.4 Optimizations	11
3.5 Material Allocation	11
3.6 Interfaces and Attachments	12
4.0 Loads and Environments, Assumptions	13
4.1 Design Load Derivations	13
4.2 Environmental Considerations	14
5.0 Analyses	15
5.1 Analysis Techniques	14
5.1.1 Analytical Tools	14
5.1.2 Developed Models	15
5.2 Performance and Sensitivity Analyses	15
5.2.1 Dynamic Thrust	15
5.2.2 Take-off and Climb-out Performance	16
5.2.3 Flight and Maneuver Performance	16
5.2.4 Static and Dynamic Stability	17
5.2.5 Payload Prediction Equation	17
5.2.6 Drag Polar Analysis	18
5.3 Structural Analyses	18
5.3.1 Applied Loads and Critical Margins	18
5.3.2 Mass Properties and Balance	19
6.0 Subassembly Tests and Integration	20
7.0 Manufacturing	22
8.0 Conclusion	23
Appendix A – Calculations and Referenced Documents	24
Appendix B – Technical Data Sheet	25
2D Drawing	26

**List of Symbols:**

c	Chord of the control surface	S	Wing Planform Area
C_d	Drag coefficient of airfoil	S1	Maximum control surface deflection
C_l	Lift coefficient of airfoil	S2	Maximum servomotor deflection
C_D	Drag coefficient of aircraft	S_{TO}	Takeoff Distance
C_{Di}	Lift-induced drag coefficient	t	Time period
C_{D0}	Zero-lift drag coefficient	T	Thrust
C_L	Lift coefficient of aircraft	v	Airspeed
C_M	Coefficient of pitching moment of aircraft	v_d	Dive speed
d	Diameter of the propeller	v_e	Exit Velocity
D	Drag	W	Weight of the aircraft
g	Acceleration due to Gravity	α	Angle of attack
L	Lift	β	Factor of correction in Thrust calculations
m	Mass of the aircraft	ρ	Density
n	Load factor	ω	Frequency
P	Payload mass	ζ	Damping Factor
q	Pitch Rate	Φ	Aircraft Bank Angle

List of Abbreviations:

CG	Centre of Gravity	MoS	Margin of Safety
FoS	Factor of Safety	TMA	Tail Moment Arm
MAC	Mean Aerodynamic Chord	UTM	Universal Testing Machine

List of Figures and Tables:

Figure 1(a)	System Overview	Table 4(b)	Landing Shock Calculations
Table 1(b)	Subsystem Details	Figure 5(a)	Dynamic Thrust Performance
Figure 2(a)	Schedule Summary	Figure 5(b)	Runway Performance
Figure 2(b)	Cost Summary	Figure 5(c)	Maximum Banking Angle
Figure 2(c)	Schedule and Cost Breakdown	Table 5(d)	Minimum Turning Radius
Figure 3(a)	Wing Layout	Figure 5(e)	Lateral Stability Eigenvalues
Figure 3(b)	Empennage Layout	Figure 5(f)	Time Response for Short Period and Phugoid Modes
Figure 3(c)	Fuselage Layout	Table 5(g)	Drag Distribution
Figure 3(d)	Electronic System Layout	Figure 5(h)	C_D at various Angles of Attack
Figure 3(e)	Weight Distribution	Figure 5(i)	Crosswind Analysis
Figure 3(f)	Ball Placement Strategy	Figure 5(j)	Composite Stress Analysis
Figure 3(g)	Planform Analysis	Figure 5(k)	Critical Margins
Figure 3(h)	C_M vs. α	Figure 5(l)	Weight Distribution
Figure 3(i)	Servo Torque Requirements	Figure 6(a)	Thrust Comparison
Figure 4(a)	V-n Diagram		



1.0 Executive Summary

1.1 System Overview and Discriminators

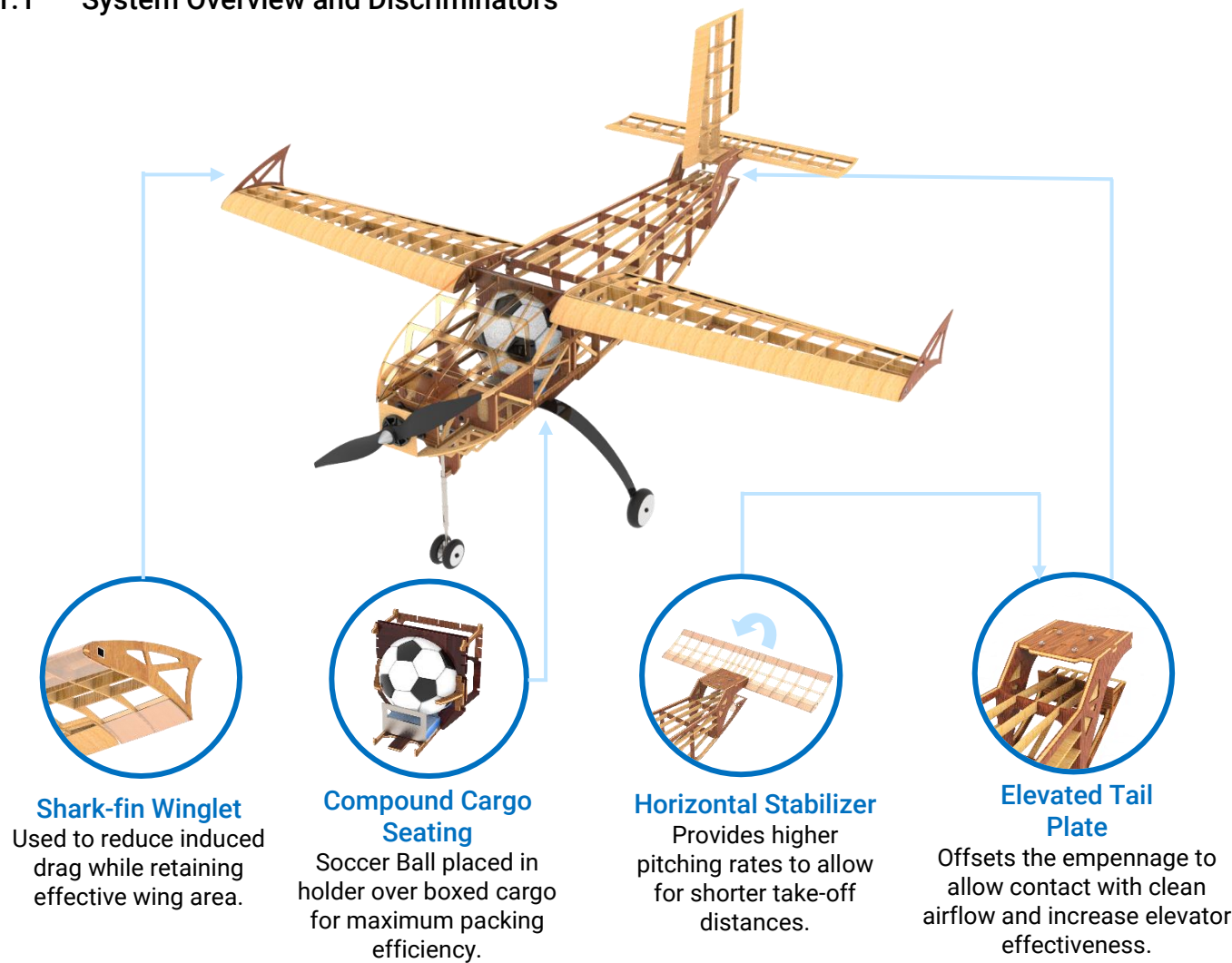


Figure 1(a): System Overview

Electronics		
Motor	Propeller	Battery
Sunny Sky X5320 250kV	APC 22x12WE	Tattu LiPo 3300mAh 6S
Wings		
Airfoil	Span	Planform
S1223 RTL	72"	Recto-Trapezoidal
Empennage		
Horizontal Tail Airfoil	Vertical Tail Airfoil	Configuration
AH79-100C	NACA0009	Inverted T Tail

Table 1(b): Subsystem Details



1.2 Competition Projections

We aim to successfully carry 12lbs. total cargo weight in the competition with a projected score of 19.26 points per round and 67.8 points in total after adding the payload prediction bonus. Combining flight scores with strong Design Report and Technical Presentation scores, we see ourselves placed in the top 5 ranks overall. After extensive testing and optimization, we are confident of its performance and reliability during the competition. The prediction is based on comparison with the top scores achieved per round in the past 3 years of SAE Aero Design.

2.0 Project Management

2.1 Schedule Summary

We started working in July with extensive testing of material alternatives, aerodynamic concepts and structural designs. We based our schedules on monthly cycles of design, testing and optimization working around our exam schedule and the annual workshop.

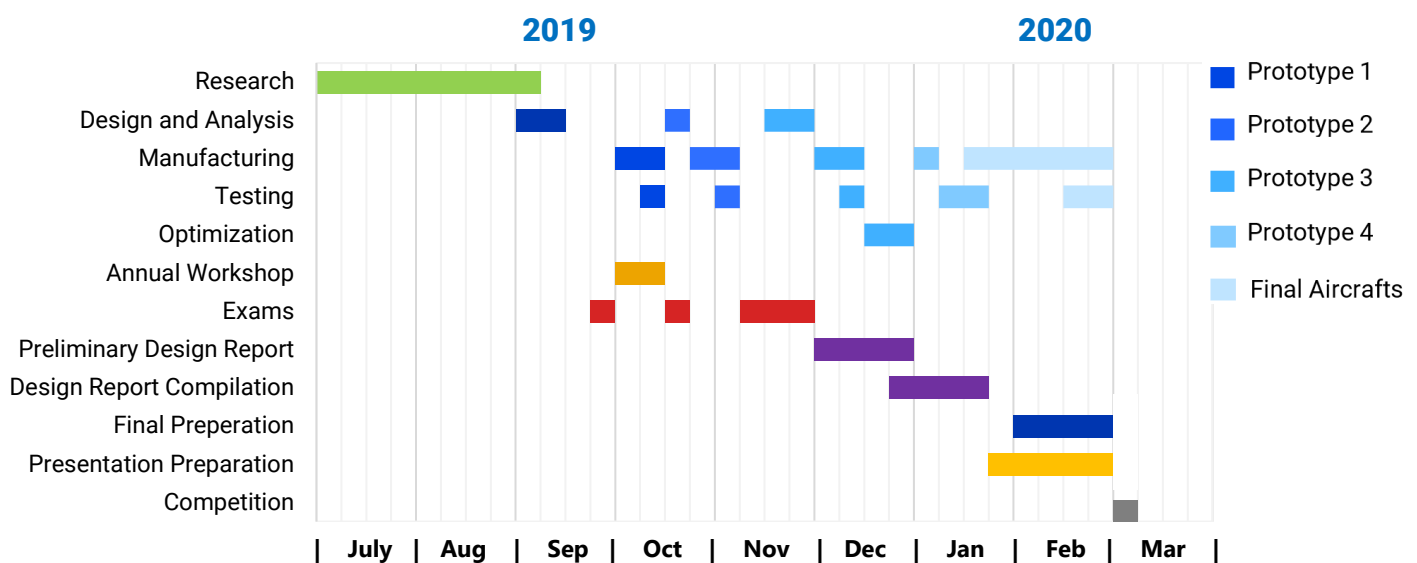


Figure 2(a): Schedule Summary

2.2 Personnel Management

Comprising of 28 students, the team was segregated into aerodynamics, structures, avionics and marketing departments. Each department had specific individuals assigned to a class while continuing to work as a single group. This ensured that ideas could be shared and discussed effectively within and in between departments, allowing progress in designs for both classes, Regular and Micro. Over time, Design Report and Technical Presentation groups were formed.

2.3 Cost Report

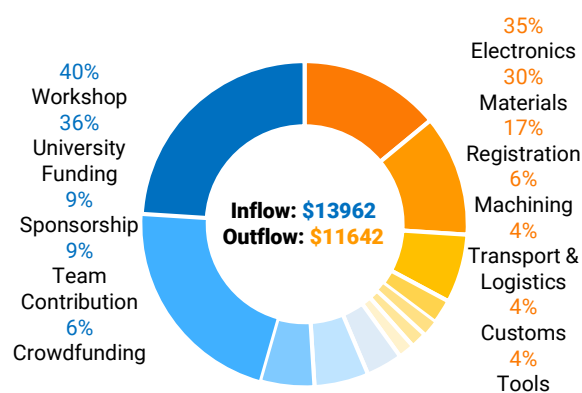


Figure 2(b): Cost Summary

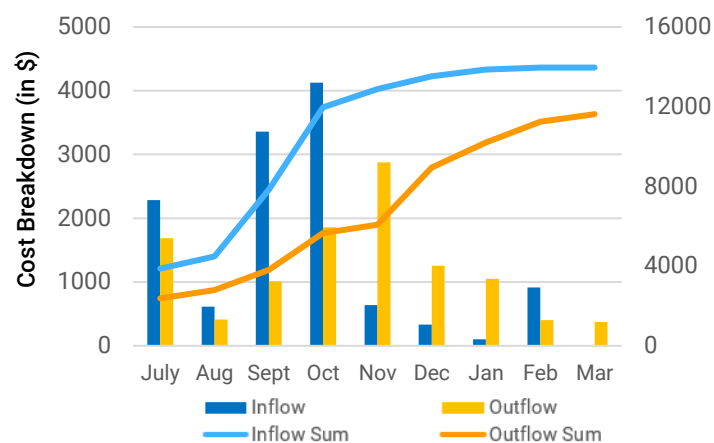


Figure 2(c): Schedule and Cost Breakdown

The outflow of funds largely comprised of electronic components, raw material procurement, manufacturing tools, registration fee and logistics. Starting with university funding received in August, we raised funds through sponsorships and crowdfunding throughout the year. In September we organized an annual aero-modeling workshop for aero enthusiasts across Mumbai to raise additional funds, ensuring sustainability. To reduce the high costs of material procurement, we contacted international wholesalers directly. Heavy customs duty and long shipping periods limited our options for testing electronics. However, we overcame this by using online tools to shortlist electronics before testing. Figure 2(c) represents how funds were managed through the year to eliminate any financial blockages in the design process and manufacturing.

3.0 Design Layout and Trades

3.1 Overall Design Features and Details

1. Wings:

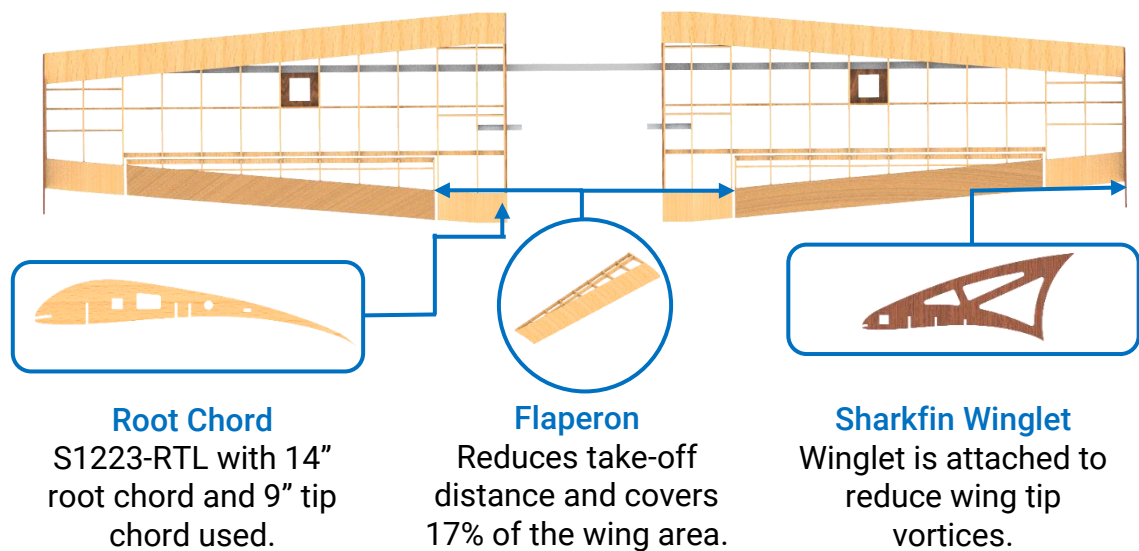


Figure 3(a): Wing Layout

We chose S1223 RTL (Selig 1223 w/Richard T. LaSalle modification) airfoil in the wing and a span of 72". The planform is recto-trapezoidal, with a rectangular region of 20% which has higher lift than a fully tapered wing while having lower induced drag as compared to a rectangular wing. We made the main spars from hollow aluminum beams with airfoil shaped ribs made of balsa. A spar towards the trailing edge is provided to retain the 5° angle of incidence during flight loads.

2. Tails:

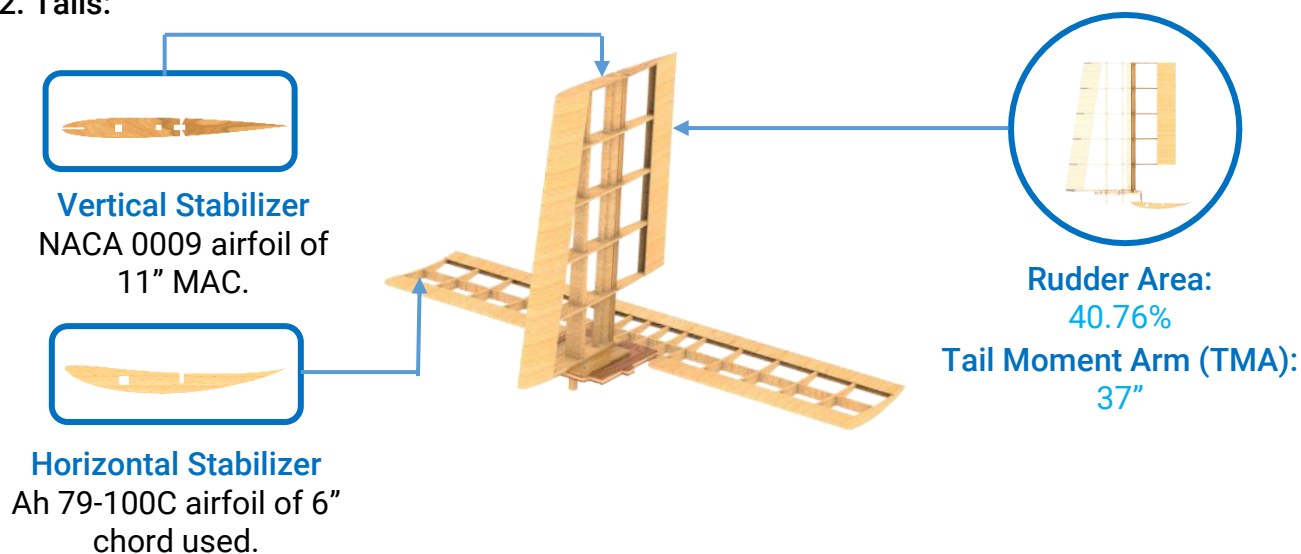
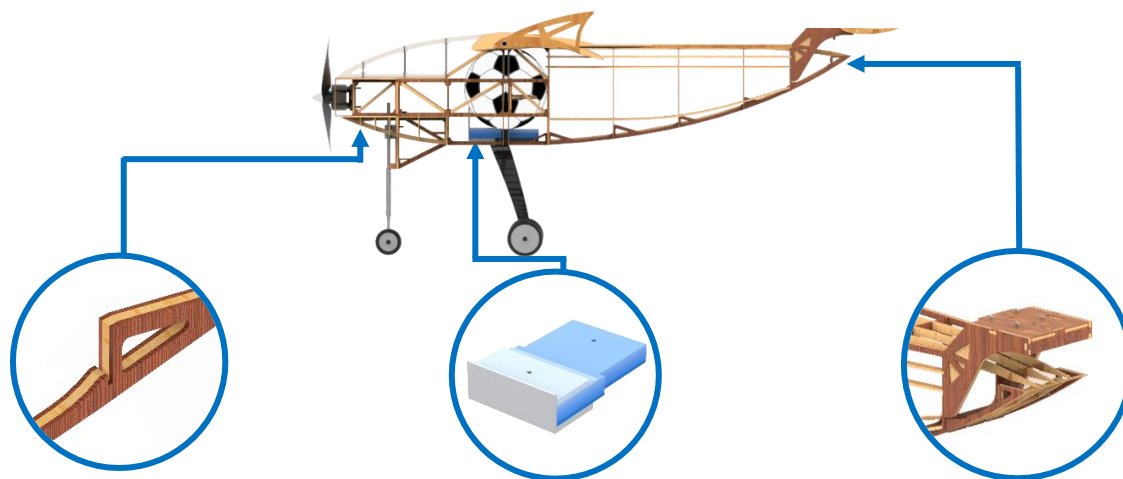


Figure 3(b): Empennage Layout

3. Fuselage:

The fuselage was designed as a chassis structure with auxiliary aerodynamic covers overlaid at strategic locations. We built the fuselage in three sections for ease of manufacturing. The tail section is tapered at the sides and curved at the bottom to reduce flow separation drag and minimize chances of a tail strike.



Composite Structure

Laminates of balsa and basswood ply used to reinforce longitudinal members.

Boxed Cargo

Stacked plates of mild steel used as boxed cargo over a common baseplate.

Empennage Vent

Airflow at the trailing edge of the fuse is allowed to pass freely through the elevator bracket assembly.

Figure 3(c): Fuselage Layout

4. Landing Gear:

We used a tricycle landing gear, owing to its immunity to ground looping and nose-overs. The main landing gear is a carbon fiber structure. The nose landing gear comprises of co-axial aluminum shafts with spring suspension. We used 3.5" diameter wheels made of rubber.

5. Boxed Cargo:

An ergonomic design for the boxed cargo aimed for the highest compactness, ease of loading and machinability. The primary dimensions were derived from the diameter of the soccer ball to minimize cargo length and maximize score. A stacked plate arrangement allowed for efficient manufacturing, handling and arrangement to allow changes in weight per flight round.



6. Spherical Cargo Seating:

The spherical cargo is placed at the mid-section and under the wing. As the boxed cargo had to be directly under the ball for maximum score and the overall CG was majorly influenced by its location, we had to place the ball near the desired loaded CG location. The ball is restricted in place with complementary structures and a buckle-strap, which allows easy removal and fitting. A detachable cover allows access to the cargo bay during loading.

7. Electronics:

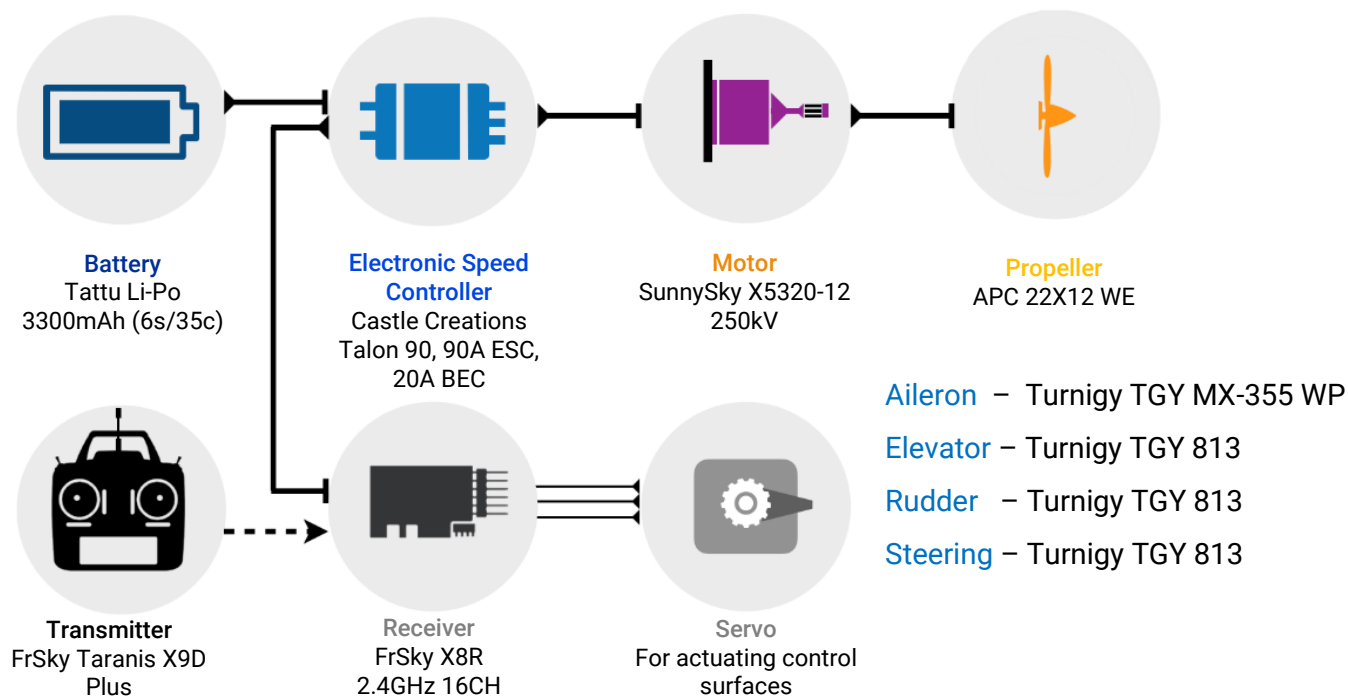


Figure 3(d): Electronics System Layout

3.2 Competitive Scoring and Strategy Analysis

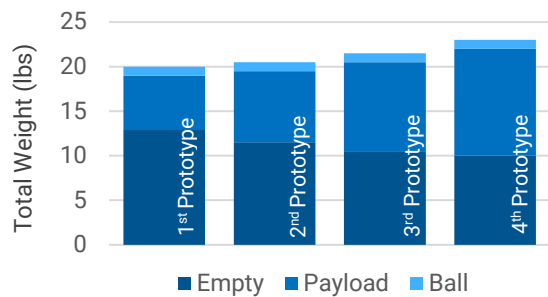


Figure 3(e): Weight Distribution

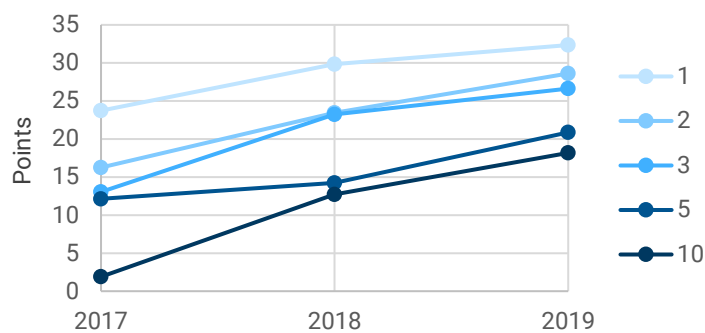


Figure 3(f): Ball Placement Strategy



The **Figure 3(f)** shows the performance progression of teams for each rank from previous SAE Aero-design events. After analyzing the trends, we set our goal for this competition which is to acquire 20 points per round, cumulating to a projected final score of 70.

As multiple configurations led to similar scores, we developed mathematical models to narrow down viable scoring strategies using surrogate modeling and genetic optimization. **Figure 3(g)** compares the performance of various spans in accordance with the scoring equation. After empirical testing we arrived at a span of 72" and an aspect ratio of 6, which was found to have the highest payload capacity. **Figure 3(e)** shows the progression of our design's multiple prototypes, where we prioritized reducing empty plane weight and increasing lifting capabilities. We had initially considered placing multiple balls laterally or vertically to optimally utilize weight but the structural and aerodynamic drawbacks proved to be unfavorable to the final scores.

3.3 Design Derivations

1. Wing:

We curated a database of multiple airfoils, differentiating them based on the parameters of minimum drag, maximum lift, maximum airfoil efficiency and maximum stall angle. Among these, we found that S1223 RTL performed the best. This was attributed to its superior stall characteristics and wing efficiency across all aspect ratios considered. We used this airfoil as a probe for initial scoring analysis, and found that a span ranging from 70"-75" with an aspect ratio between 5.5 - 6.5 gave the highest scores. We used the previous year's design and performance data to verify our scoring trend in a practical setup before moving forward.

3 recto-trapezoidal wing planforms each with an aspect ratio of 5.5, 6.5 & 6 were practically tested in subsequent prototypes. Root chord and tip chord pairs of 14" & 9" and 13" & 8", were considered. An angle of incidence of 5° maximized the wing efficiency and improved take-off and flight performance of the design.

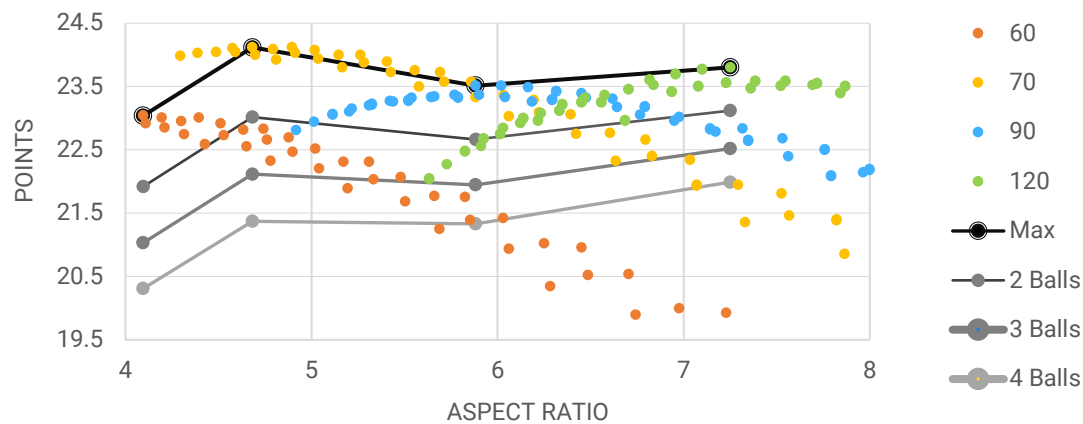


Figure 3(g): Planform Analysis

The wing designed for the 3rd prototype was judged as the best performing wing from flight test data. This is attributed to its optimized area which reduces drag and subsequently better acceleration than the 1st prototype and better runway performance than the 2nd prototype. We added flaperons to reduce take-off distance. Even with reduced wing efficiency, ground friction is minimized and take-off distances are lowered.

The 4th prototype emphasized induced drag optimization using wingtip devices. We compared a variety of Winglets and Hoerner tips. The former was chosen as it restores otherwise lost lift while increasing the effective Aspect Ratio of the wing.

2. Fuselage:

The primary dimensions of the fuselage were derived from the required TMA, CG position, avionics and cargo bay lengths. To reduce the drag penalty on the fuselage, the frontal area and length of the mid-section were minimized. UTM testing and topology optimization tests were performed on critical load bearing components to ensure an appropriate MoS. A truss structure was implemented for the mid-section to withstand impact loads while a semi-monocoque structure was followed in the tail section to resist bending moments and maintain outer mold line till the empennage. A top loading approach was followed as trusses are not present in the



horizontal plane. The tail section is tapered by 5.5° on two sides and curved at the bottom, reducing fuselage generated drag by 21.3%.

3. Horizontal Stabilizer:

To achieve a favorable empty weight & CG position and to counter structural limitations, we used an asymmetric airfoil, AH 79-100 C, for the horizontal stabilizer. A stabilizer was used over the conventional horizontal tail with elevator, as it allowed for greater pitching moments and take-off at marginally lower velocities.

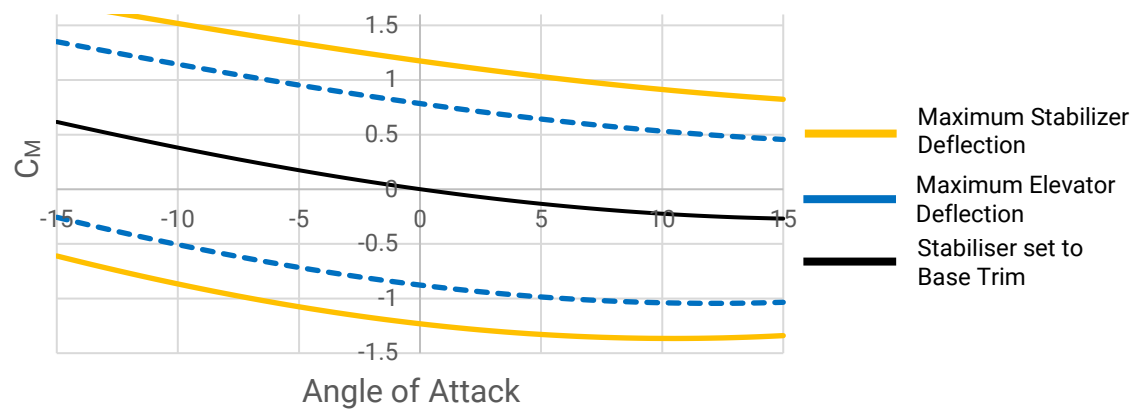


Figure 3(h): C_M Vs α

4. Vertical Tail:

NACA 0009, a symmetric airfoil, was selected for its low drag at 0° angle of attack. The area was calculated using a tail volume coefficient of 0.3 with a TMA of 37.4” available. The root chord 12” and tip chord 10” were derived from the operating Reynolds Number.

5. Electronics:

Control Surface	Servomotor	Rated Torque (oz-in)	Control Surface Deflection	Required Torque (oz-in)
Flaperon	Turnigy MX355WP	166.6486387	30°	41.9
Elevator	Turnigy 813	124.986479	30°	100.3
Rudder	Turnigy 813	124.986479	30°	52.3
Nose Landing Gear	Turnigy 813	124.986479	30°	52.3

Figure 3(i): Servo Torque Requirements



The selection of motor and propeller was based on dynamic performance analysis for various flight conditions of take-off, turning and cruising. The required torque at the control surface hinge was calculated as mentioned in Appendix A, at the dive speed of the aircraft. The servo torque at the hinge was found out as the servo arm and control horn lengths were known.

3.4 Optimizations

We utilized a telemetry logging network situated at the avionics bay, which included a variety of sensors and data-logging equipment. ArduPilot Mega (APM) was used to coordinate flight patterns and log data from sensors placed at strategic locations in the aircraft.

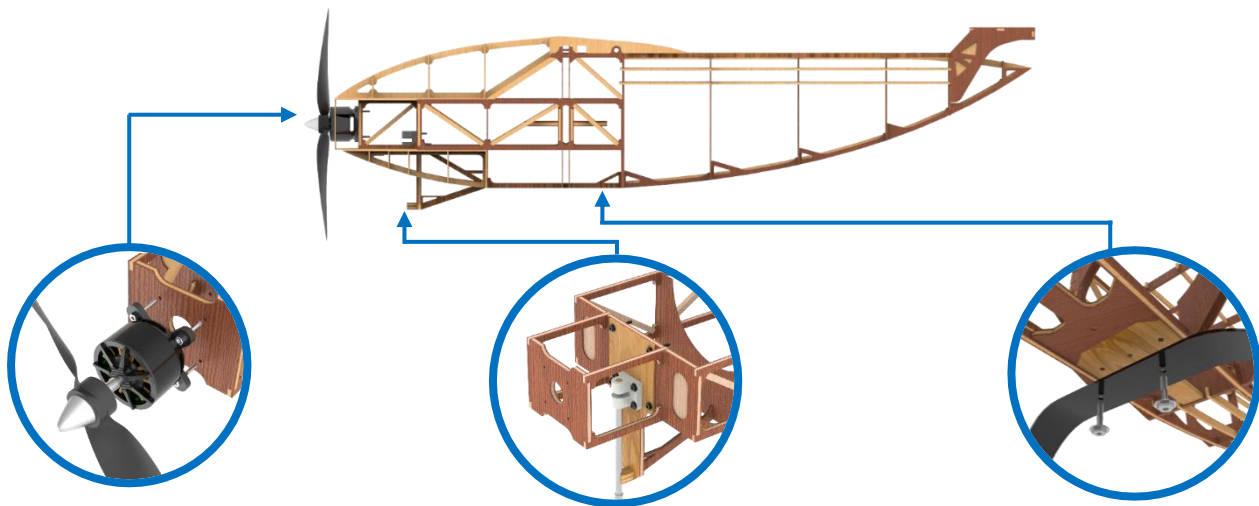
We performed extensive testing of material alternatives and longeron cross-sections, preferring higher strength to weight ratio within the desired MoS. Topology optimization tools were used to accurately arrive at optimized structures with the desired MoS of 20% which reduced component weight by up to 28%. Triangular gusset plates were added to maximize contact surface in critical load-bearing elements such as landing gear plates and in Warren trusses along with filleted junctions to aid in the dispersion loads. Struts for nose landing gear were added to preserve integrity during impact loads, besides it being replaceable in case of system failure.

3.5 Material Allocation

We constructed the airframe primarily with wood, with the main wing spars being made out of aluminum due to its anisotropic strength and high endurance. A hollow square cross-section aluminum beam is used for its higher strength to weight ratio. Balsa was used in the wing and tail sub-assemblies for its low density and high strength to weight ratio. We used basswood ply at regions of higher concentrated loads, namely near the landing gears, wing and tail junctions. Laminates of balsa and basswood ply were used for the remainder of the design as they offer significantly higher strength than balsa helping strengthen critical areas all while being much lighter than conventional hardwood.

3.6 Interfaces & Attachments

FUSELAGE



Motor Mounting

The firewall made from laminate of basswood ply and balsa is used to attach the motor to the fuselage.

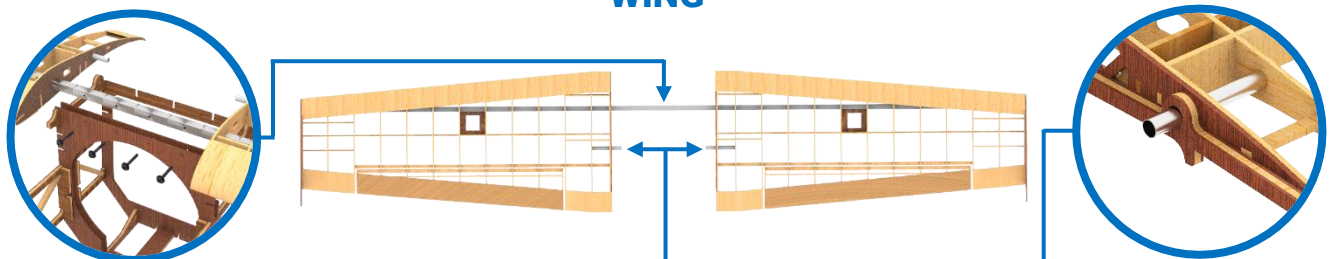
Nose Landing Gear Mounting

A Delrin bush mounted on a modular plate is used to attach the nose landing gear to a thick laminate rib.

Main Landing Gear Mounting

Landing gear bolted to a thick composite baseplate in the lowest deck of the fuselage.

WING



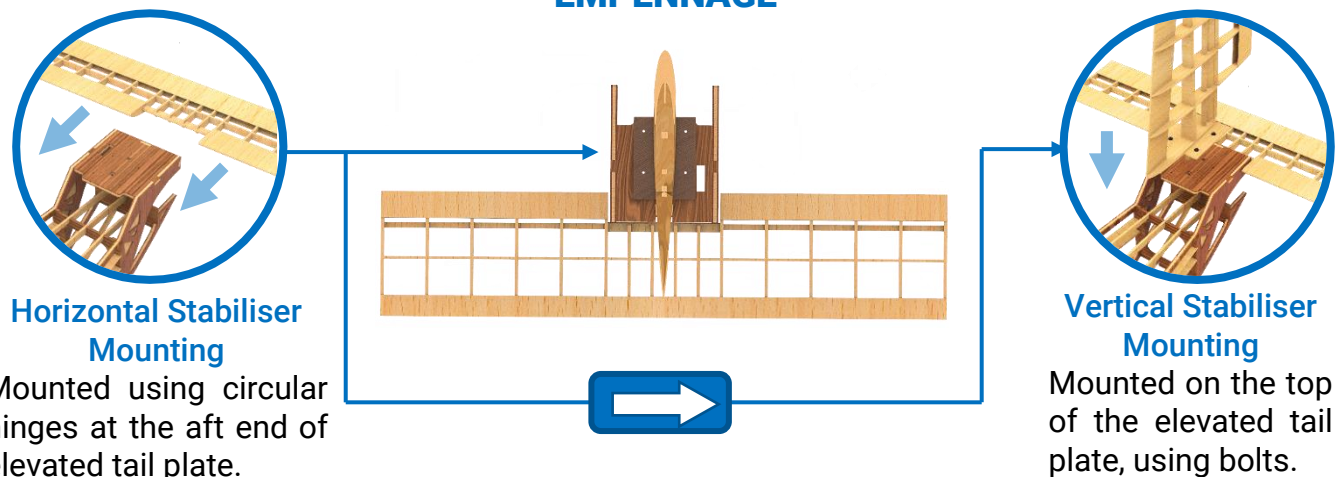
Primary Spar Locking

Bolting through co-axial holes in plywood formers of the mid-section on aligning with the primary spar.

Rear Spar

Hollow aluminum rod passed through the wing root section and into longerons.

EMPENNAGE



Horizontal Stabiliser Mounting

Mounted using circular hinges at the aft end of elevated tail plate.

Vertical Stabiliser Mounting

Mounted on the top of the elevated tail plate, using bolts.



4.0 Loads, Environments and Assumptions

4.1 Design Load Derivations

1. V-n Diagram

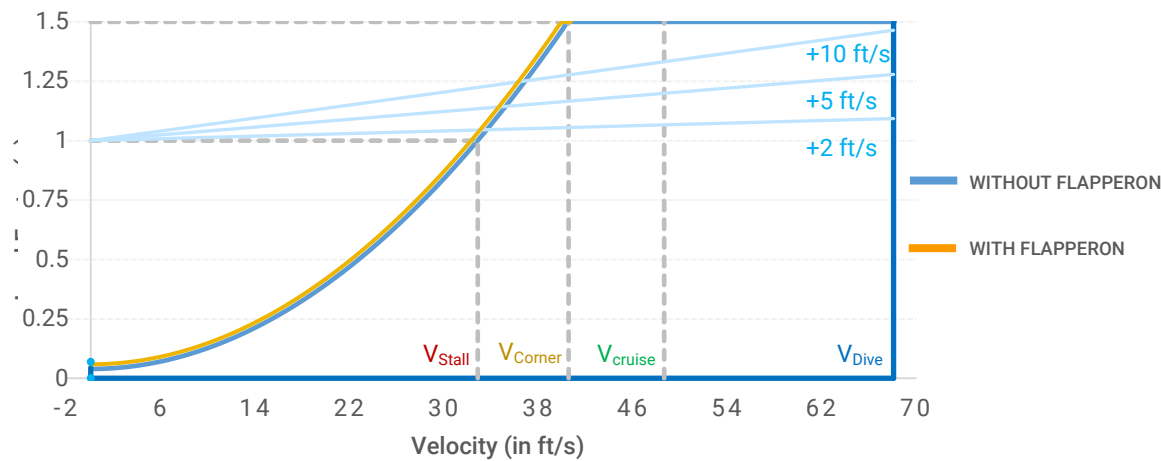


Figure 4(a): V-n Diagram

Figure 4(a) depicts the V-n diagram for our aircraft. A non-zero load factor is produced when the aircraft is stationary as lift is generated at the wing due to the effect of prop wash. The flight envelopes for wing configuration with flaperons have been analyzed as well. Only positive load factors have been considered as the airplane is not designed to fly inverted.

2. Landing Shock

Glideslope (°)	Sink Rate (ft/s)	Impact Loading (lbf)
3	1.94	27.99871
5	3.231	32.40795
10	6.437	43.15769

Table 4(b): Landing Shock Calculation

We calculated the impact loading on the airframe during touchdown by calculating change in momentum and normal force. We used accelerometer data to accurately predict the former and assumed approach velocity to be equivalent to stall speed. The median impact time was recorded as 0.2 seconds from multiple flight tests. Glideslopes of 3°, 5° and 10° were considered.



4.2 Environmental Consideration

Mumbai is subjected to calmer weather. Based on previous experiences, we noted the gusty wind conditions of the competition site and tested our aircrafts at similar locations in India. This was done to ensure the aircraft's performance in competition. The air density change was also accounted, with Mumbai having 0.0728 lb/ft^3 during the testing phase and Lakeland having 0.0755 lb/ft^3 during the competition. We predicted a 4% increase in the performance of the design.

5.0 Analyses

5.1 Analysis Techniques

5.1.1 Analytical Tools

We used various analytical tools to design and optimize our aircraft to obtain the desired performance.

1. Solidworks

Flow simulation was used to compare design iterations for highest system efficiency, along with using techniques of dynamic meshing and inflation to compare boundary layer separation and effectiveness of drag reduction devices.

Topology optimization techniques were used to achieve the highest overall strength to weight ratio, and provide insight into system level structural inadequacies.

It was also used for accurately predicting the center of gravity and for mass balancing.

2. XFLR5

XFLR5 was used to obtain airfoil polars. It is also used for the stability analysis of the system, to determine longitudinal and lateral dynamic stability eigenvalues.

3. MATLAB & Microsoft Excel

Used for analyses and optimization of system variables using advanced techniques of surrogate modelling and genetic optimization to reach the desired efficiency. They were used to formulate and plot optimum strategies for scoring, runway performance and flight stability.

5.2 Developed models

To accurately predict the velocity of the aircraft on the runway and the take-off distance, we used differential equations with velocity-dependent parameters of dynamic thrust, friction and drag while keeping displacement as the primary variable.

For turning flight, we analyzed the free body diagram of our aircraft while banking. Horizontal and vertical components of lift were equated to centrifugal force and weight respectively. After simultaneously solving these equations, we obtained the maximum angle of bank and minimum turning radius.

With reference to Section 3.4, optimization models like surrogate modelling and genetic analysis were used to narrow down scoring strategies. We also developed a model for dynamic thrust, which utilizes propeller air ejection velocity and static thrust values to estimate dynamic thrust.

5.2 Performance and Sensitivity analysis

5.2.1 Dynamic Thrust

We analyzed the dynamic thrust characteristics of various motor propeller combinations, as described in section (6.0). Figure 5(a) compares three best combinations.

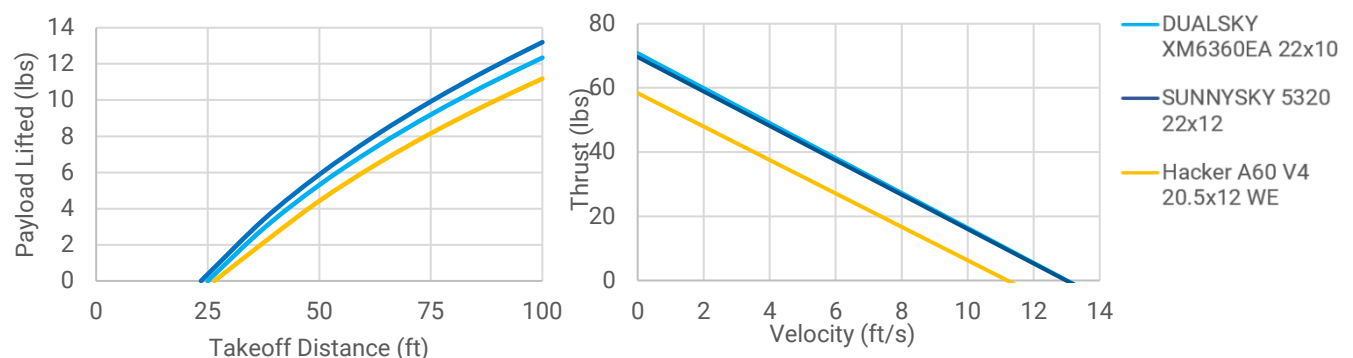


Figure 5(a): Dynamic Thrust Performance



5.2.2 Take-off and Climb-out Performance

We developed a model to analyze take-off performance with varying payload weight, under different weather conditions. Empirically obtained values are plotted for reference. Some deviation is expected as we assumed consistent angle of rotation.

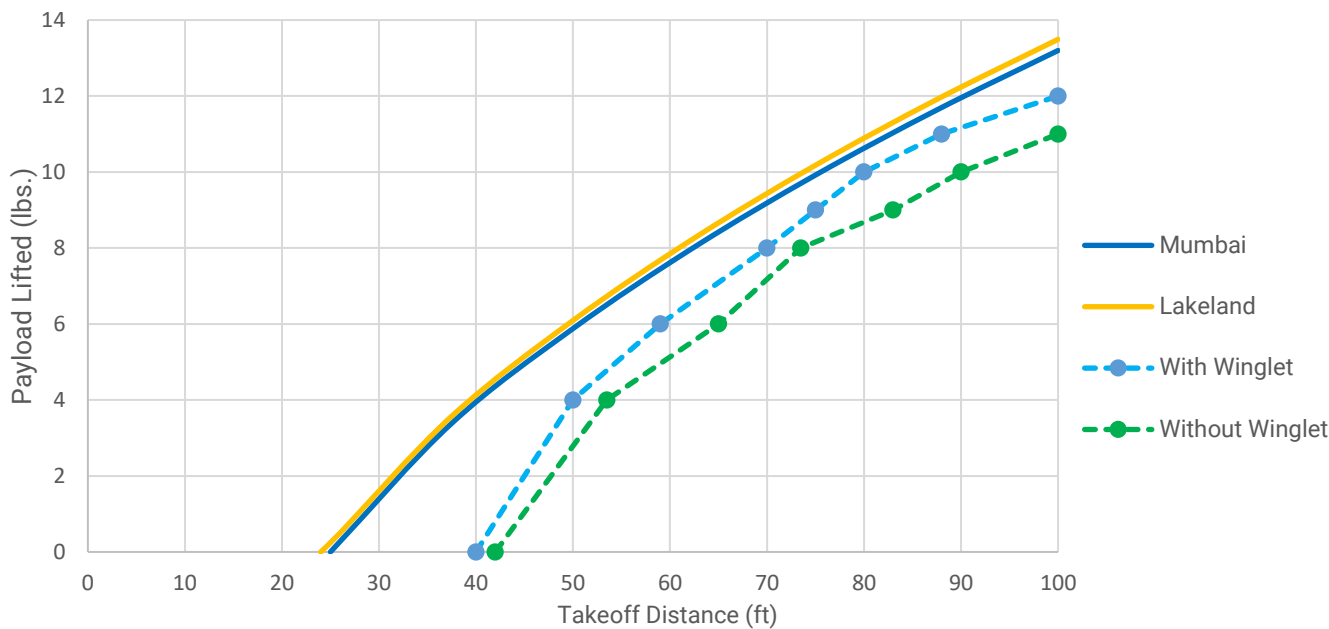


Figure 5(b): Runway Performance

5.2.3 Flight and Maneuver Performance

We calculated the maximum angles of banking and minimum turning radii for varying payload weights, according to the model described in Section 5.1. The corresponding values are plotted below.

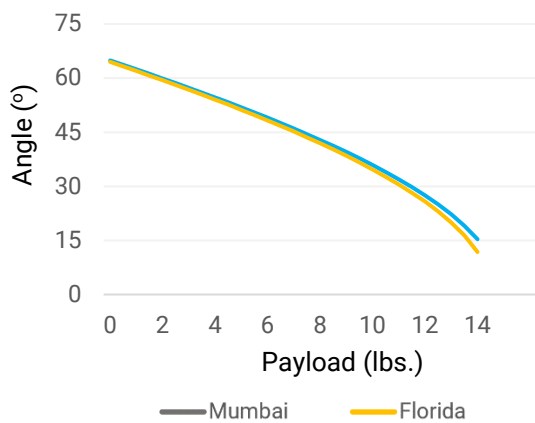


Figure 5(c): Maximum Banking Angle

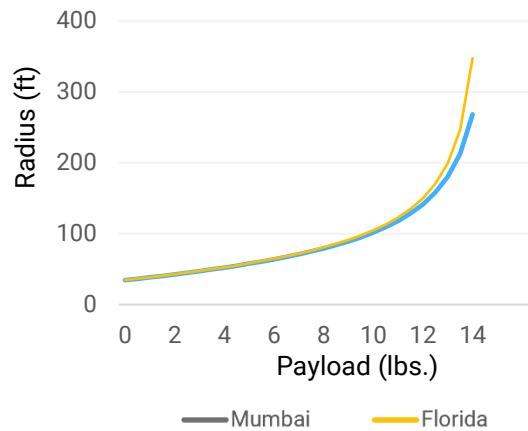


Figure 5(d): Minimum Turning Radius



5.2.4 Static and Dynamic Stability

The negative slope of Inverted AH 79-100C airfoil curve in **Figure 3(b)** indicates that the aircraft is statically stable. The neutral point is 19.23” from the aircraft datum and the static margin is 25.57% of Mean Aerodynamic Chord. Dynamic stability of the aircraft was analyzed using Stability Analysis on XFLR5. Listed below are the Lateral Stability Eigenvalues for the aircraft:

Roll Dampening	-26.3	Dutch Roll	- 5.438+10.62i	Spiral Instability	0.3427
----------------	-------	------------	----------------	--------------------	--------

Table 5(e): Lateral Stability Eigenvalues

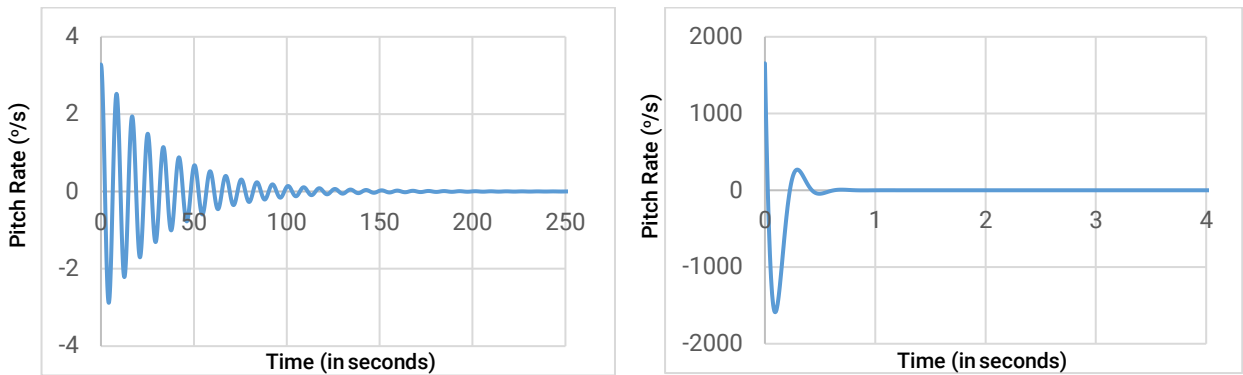


Table 5(f): Time Response for phugoid and short period modes

Longitudinal Stability: The above graphs depict the time response of the aircraft about the lateral axis in pitch rate (degrees/second) versus time (seconds). The damping factors and times of oscillation being 0.278 and 0.29 seconds for Short-period mode, and 0.041 and 8.4 seconds for Phugoid mode respectively.

5.2.5 Payload Prediction Analysis

The change in the aircraft’s lifting capability is calculated by using the following equations:

$$L = n(m_{empty} + m_{payload}) ; 0.5SC_L v^2 \rho = n(10g + P_g) ; P = K\rho - 10$$

[Where constant $K = SC_L v^2 / 2ng$]

On inputting $\rho = 0.0765 \text{ lbs/ft}^3$; $m_{empty} = 10\text{lbs}$; $m_{payload} = 12\text{lbs}$; $T = 59^\circ\text{F}$ and $P = 14.6959488 \text{ psi}$ at ground level in accordance with International Standard Atmosphere values, $K = 287.582$.



After correlating air density with altitude using temperature and pressure relations, the payload prediction vs density altitude curve obtained is of the equation:

$$[y = -0.00064x + 12]$$

[where y = Payload(lbs); and m = Altitude(ft)]

5.2.6 Drag Polar Analysis

We calculated the drag contributions of individual components over 3 prototypes using [2]. The results are tabulated in as shown below.

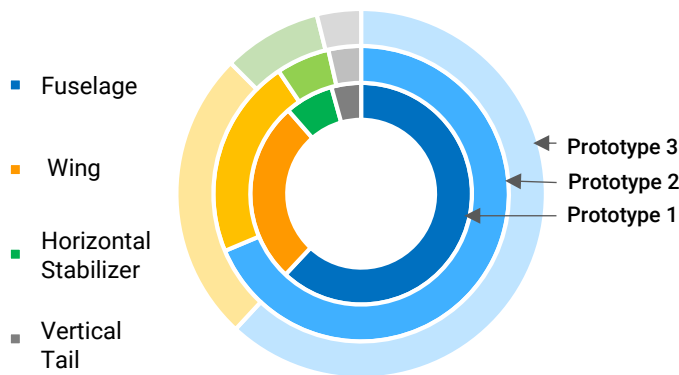


Figure 5(g): Drag Distribution

α	C_{D0}	C_{Di}	C_D
0°	0.0227	0.1003	0.1230
2°	0.0227	0.1238	0.1466
4°	0.0227	0.1492	0.1719
6°	0.0227	0.1745	0.1973
8°	0.0227	0.2023	0.2251
10°	0.0227	0.2311	0.2539

Table 5(h): C_D at various Angles of Attack

5.3 Structural Analyses

5.3.1 Applied Loads and Critical Margins

1. Tail Force Analysis:

We analyzed rudder performance under crosswind conditions. A mathematical model was developed to measure rudder forces based on crosswind intensity, we found that rudder becomes completely ineffective at 17.5 ft/s.

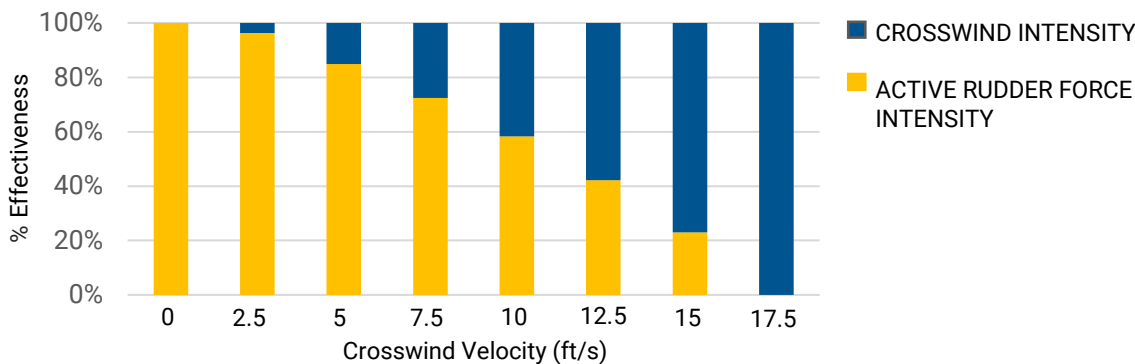


Figure 5(i): Crosswind Analysis



2. Elevator Bracket

An elevator bracket was added to facilitate a clean airflow to the empennage. Two laminated plates were used for the same. We ran stress analyses on the section to ensure it could withhold the maximum applied loads. The first iteration was tested with balsa but it failed before meeting the required FoS. Composites of basswood and balsa were used for the next iteration which were ultimately selected.

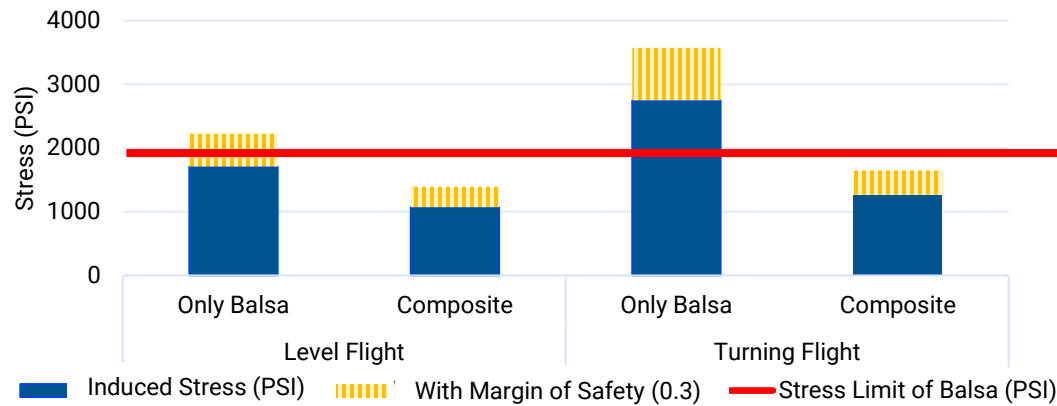


Figure 5(j): Composite Stress Analysis

3. Critical Margins

Material	Location	Max Stress induced (PSI)	Max Allowed Stress (PSI)	FoS
Balsa	Stringers	1576.4	1914.5	1.214
Basswood	Base Plate	1199.8	2552.7	2.3
Aluminium	Wing Dowel	11852.5	26933.5	2.272
Mild Steel	Wing Locking	33086.6	57989.9	1.752

Table 5(k): Critical Margins

5.3.2 Mass Properties and Balance

1. Centre Of Gravity

To ensure the static stability, we placed the CG in front of the Neutral Point. Based on our calculations and pilot inputs, the aircraft was designed with the CG 2.33” in front of the Neutral Point. The main landing gear was placed near the CG to aid in equal weight distribution, and prevent excessive loading on the nose landing gear.



2. Weight Distribution

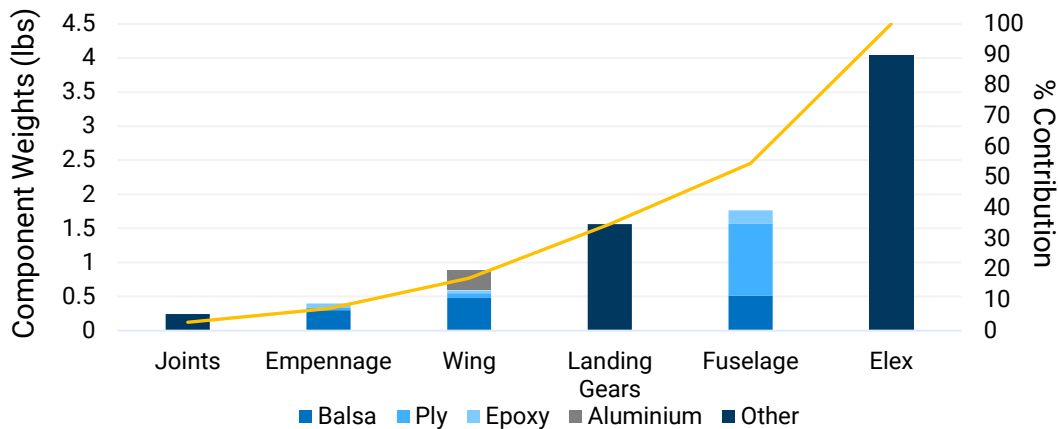


Table 5(I): Weight Distribution

3. Ball Placement Strategy

For maximum scoring with the chosen configuration, the boxed cargo will have to be placed directly under the ball and dimensionally restricted by its diameter therefore any change in ball position will majorly influence CG, so the ball was placed near the desired CG location and under the wing.

The ball is loaded diagonally from the top after placing the boxed cargo so as to reduce the required mid-section volume and thereby the weight and drag penalties.

6.0 Sub-assembly Tests and Integration

1. Propulsion System Testing

Motors of kV rating 220, 250 and 295 were acquired for testing. These were shortlisted after comparing static thrust data from an online calculator, eCalc, limiting them to 1000 watts. The dynamic thrust performance was evaluated using the values sourced from APC propeller performance data sheets, after which the options were further narrowed down.

We recognized the importance of static and dynamic thrust and performed empirical testing to identify sensitive parameters, including air ejection velocity and RPM. We tested the dynamic thrust using a wind tunnel. To measure thrust we used a load cell mounted vertically on a

pedestal. The motor mount was attached to the free end of the load cell, the data was calibrated and logged using Arduino UNO. All the propellers are APC propellers.

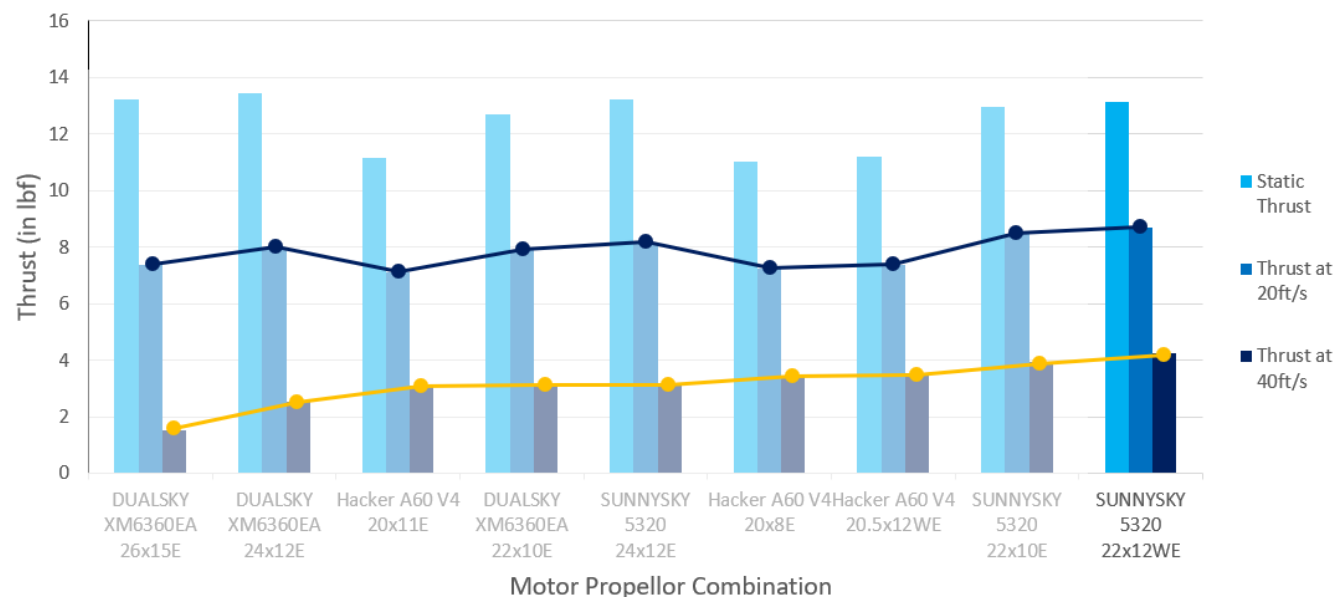


Figure 6(a): Thrust Comparison

2. Servo testing

The torque produced at the hinge depends on servo arm and control surface sizing, so we constructed an apparatus to measure the torque available at the hinge for their different lengths.

3. Battery Testing

Battery endurance was tested by operating the motor statically at full throttle for the time taken to complete 2 flight rounds. Once it endured the static test, we cross verified the battery usage during flight test for the same scenario.

4. CG Testing and Verification

Aircraft stability is highly sensitive to the position of CG with the respect to the neutral point. The manufactured model was tested for verification of the CG position with its designed position. Its effect of static loading on the nose & main landing gears and the necessary tail force in dynamic conditions was also analyzed and verified. Pilot inputs were used as a feedback for fine-tuning of the tail deflection.



5. Flight testing

Various configurations of the wing and fuselage were tested. Sensors including RPM (Rotations Per Minute) sensor, GPS (Global Positioning System) sensor, accelerometer, Pitot tube, and altimeter were incorporated in the telemetry. Flight rounds were conducted with an incremental weight buildup strategy, with the maximum lifting capacity judged from pilot feedback. We used the data gathered at flight tests to design the aircraft towards having lower take-off distances and higher lifting capacities.

6. Materials and Loads Testing

UTM tests were performed for various longeron cross-sections, alternative materials and structures to identify ultimate and shear stress values for the composites developed on the basis of base materials and cross-section. Structural loading at critical junctions was calculated to design structural members. Topology optimization tools were used to provide insight into material reduction strategies. This allowed us to save up to 28% component weight and around 8% cumulative weight while keeping 0.3 as MoS.

7.0 Manufacturing

We manufactured the aircraft by overlaying individual components on scale prints in a logical order. Laser cutting was used to cut formers, longerons, spars, wing and tail ribs for maximum accuracy. CNC (Computer Numerical Control) machining was used to make the boxed cargo, nose landing gear shafts, and nose landing gear mounting.

In wings, tails and control surfaces, multiple spars were provided with slots that fit into corresponding slots provided in the ribs, thereby acting as internal jigs as well as spars. The leading edge was given the desired contour by folding balsa sheets, which helped us reduce weight.



Laser cut formers and longeron parts were laminated using two-part resin epoxy by incrementally adding layers based on the load applied on the component, as elaborated in **Section 3.3**. We designed jigs made from acrylic to maintain alignment over the long curing time. Cyanoacrylates were used to attach balsa parts for their short curing time. Jigs were also developed to hold the curved tail-section in place during mating with the mid-section. To prevent dips, maintain the outer mold line and provide greater surface for applying the covering film, t-sections of Balsa were used. Epoxy Resin Weight was calculated by weighing components before and after application, then finding the difference. Weight reductions were done in components with lesser critical loading, and subsequently added in regions requiring higher FoS, namely the control surfaces.

8.0 Conclusion

As per the report above, we have designed an aircraft which is capable of carrying 1 spherical cargo and 11lbs of boxed cargo. We have used unique combinations of materials to ensure structural soundness, as well as performed extensive empirical testing to back our calculations. We hope to make the most of the opportunity the competition provides us, and be competitive against teams from around the world at SAE Aero Design East 2020.

References:

1. Anderson, John D., "Introduction to Flight: Its Engineering and History."
2. Caughey, David A., "Introduction to Aircraft Stability and Control Course Notes"
3. Nicolai, Leland M. and Grant Carichner., "Aircraft Design"
4. Sadraey, Mohammad H., "Aircraft Design: A Systems Engineering Approach"
5. Team 029, DJS Skylark Regular Class Design Report, SAE Aero Design West 2019.



Appendix A – Backup Calculations

Servo Calculations: (SECTION 3.2.2)

$$\text{Servo Torque Required} = (8.5 \times 10^{-6}) \frac{c^2 \times v_d^2 \times \text{control surface span} \times \sin^2(S_1)}{\cos(S_1) \times \tan(S_2)} \times \frac{\text{control horn height}}{\text{servo arm length}}$$

Thrust Calculations: (SECTION 5.2.1)

$$T = \rho \frac{\pi d^2}{4} (v^2 - v_e v) \beta = 0.28599 \times (52.493 - v) \times 0.763627$$

Take-off and Landing Analysis: (SECTION 5.2.2)

$$v^2 > \frac{mg}{\frac{1}{2}\rho S C_L} \quad \dots (1)$$

$$\text{Thrust} - \text{Drag} - \text{Friction} = \text{Mass} \times \text{Acceleration} = mv \frac{dv}{dx} \quad \dots (2)$$

$$S_{TO} = \int dx = \int \frac{mv dv}{\{T(v) - [D(v) + \mu(W - L(v))]\}}$$

The take-off distance is the value of x obtained after integrating (2), for the velocity obtained from equation (1).

Turning Radius Calculations: (SECTION 5.2.3)

$$\phi = \cos^{-1} \left(\frac{W}{L} \right), \text{ Radius of turn} = \frac{mv^2}{L \sin \phi}$$

Damping Factor: (SECTION 5.2.4)

$$\zeta = \frac{1}{\sqrt{1 + \left(\frac{2\pi}{\delta} \right)^2}} \quad \text{where} \quad \delta \triangleq \ln \frac{x_1}{x_2}$$

Where x_1 and x_2 are the vibration amplitudes at two successive peaks of the decaying vibration and δ is the logarithmic decrement.



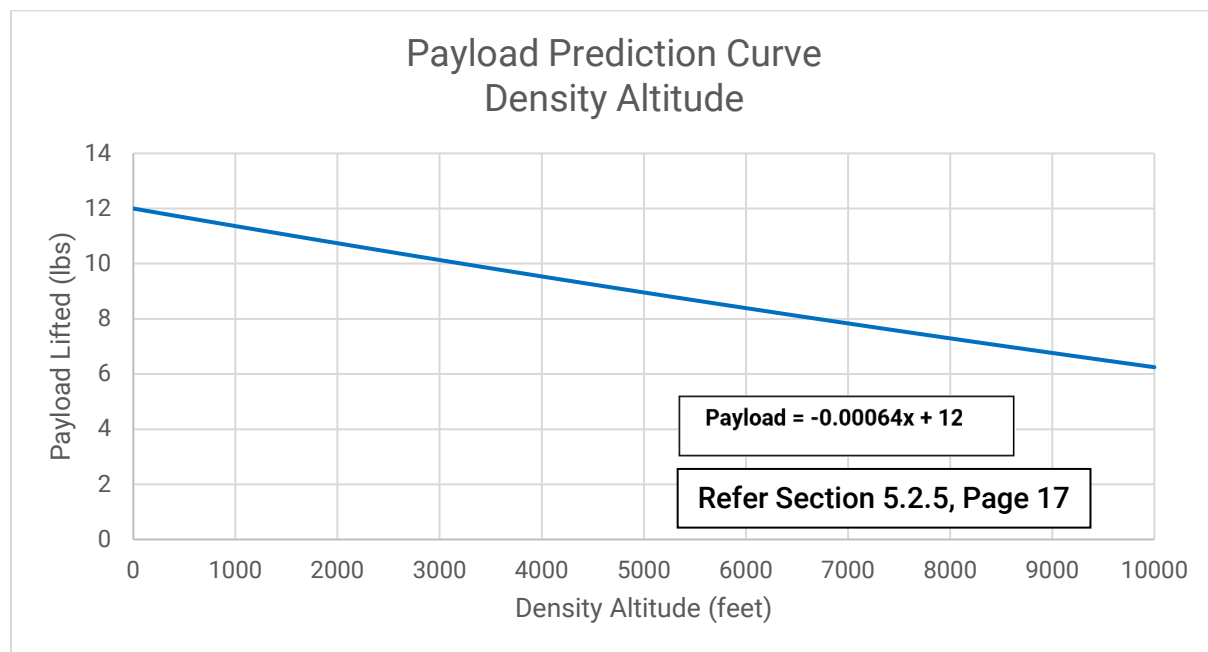
Appendix B – Technical Data Sheet

Payload Prediction Curve (Regular Class)

Team Name: DJS Skylark - Regular Class

Team Number: 024

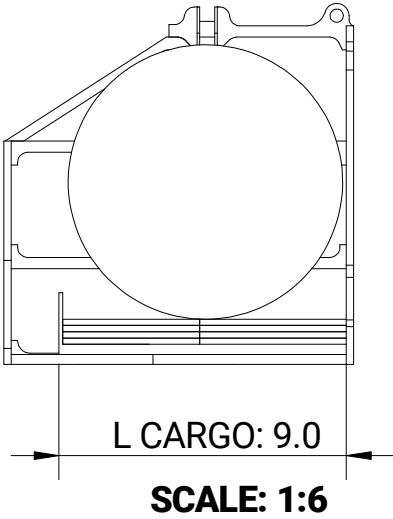
School Name: Dwarkadas J. Sanghvi College of Engineering



AIRCRAFT SUMMARY DATA

WINGSPAN	MAC	TMA	EMPTY WEIGHT	BATTERY	MOTOR MODEL	MOTOR KV	PROPELLER	SERVO (NOSE LANDING GEAR) (A)	SERVO (Aileron) (B)	SERVO (ELEVATOR) (C)	SERVO (RUDDER) (E)
72 ± 0.1"	12.22"	37.4 ± 0.1"	10.3 lbs	Tattu 3300mAh 6S 35C (22.2V) LiPo	Sunnysky X5320-12 14 Poles	250KV	APC 22x12WE	Turnigy TGY 813 (124.99oz-In)	Turnigy MX-355 WP (319.40 oz-in)	Turnigy TGY 813 (124.99oz-In)	Turnigy TGY 813 (124.99oz-In)

FULLY LOADED CARGO BAY

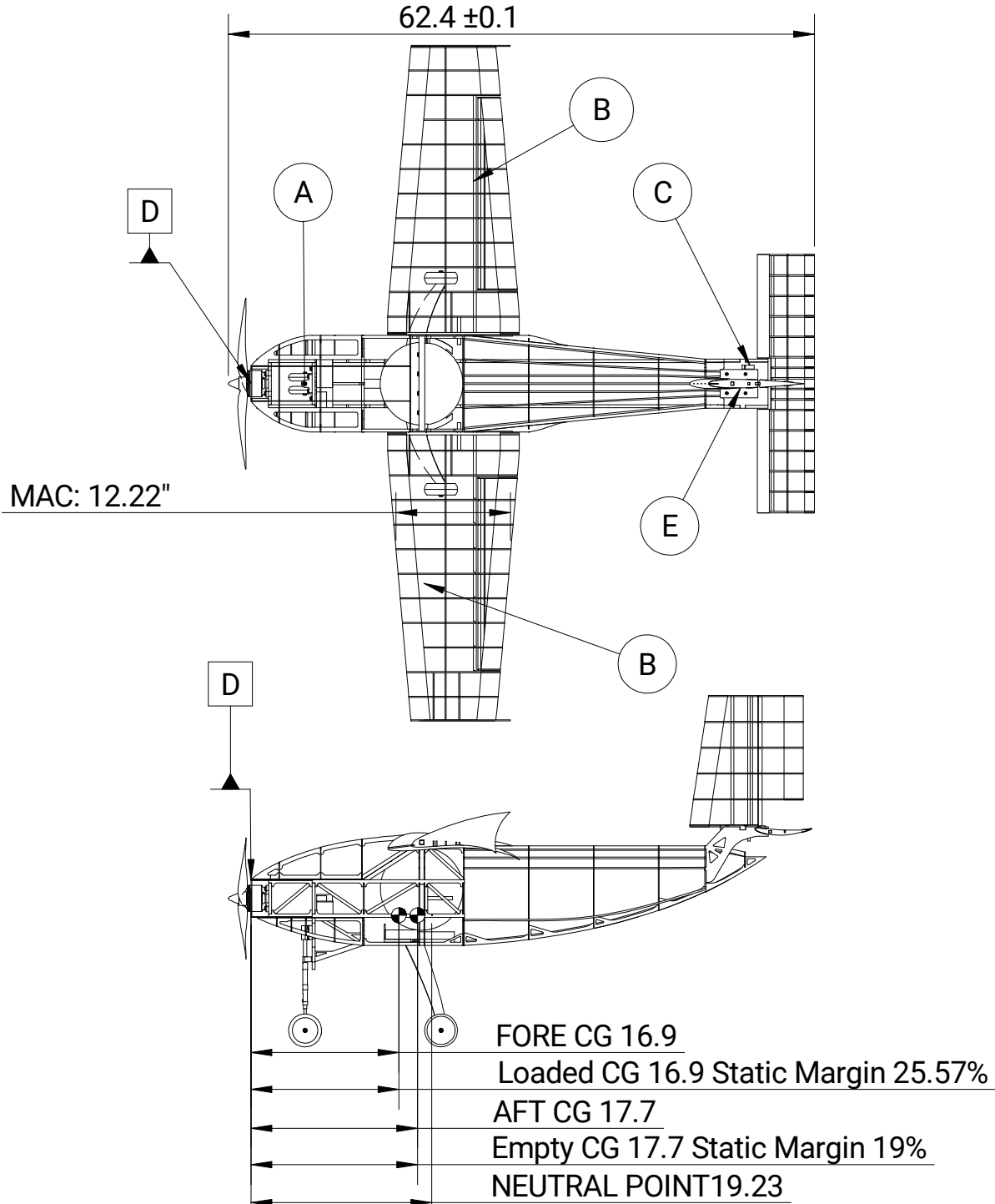
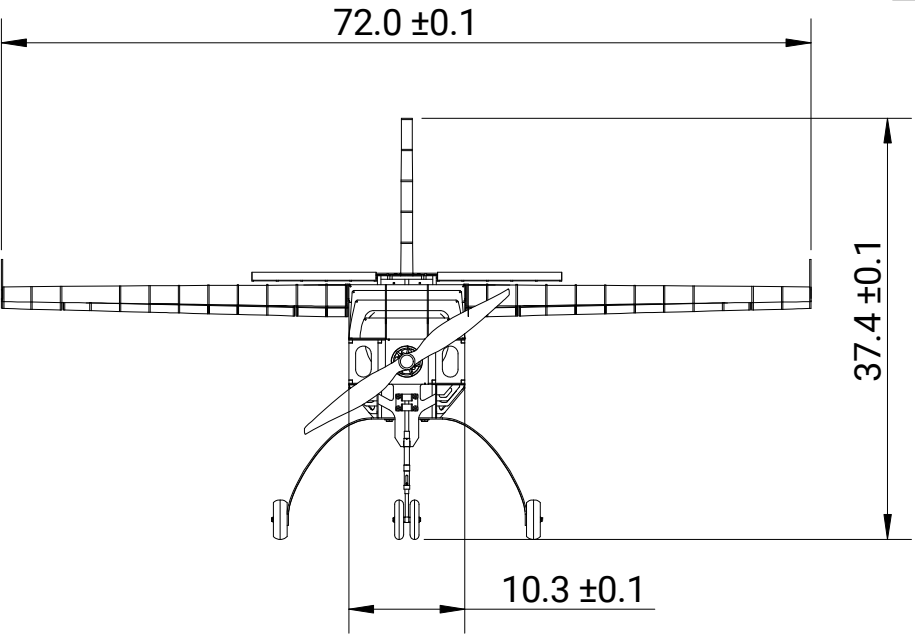


WEIGHT AND BALANCE TABLE

SR NO.	COMPONENTS	WEIGHT (lbs)	ARM (in)	MOMENT (lbs-in)
1	MOTOR	1.287	0.6794	0.875
2	BATTERY	1.268	7.6735	9.727
3	PAYLOAD	11.050	17.461	192.941
4	ELECTRONICS	1.488	17.786	26.468

BASIC DIMENSIONS

LENGTH	62.4 ± 0.1"
WIDTH	72 ± 0.1"
HEIGHT	37.4 ± 0.1"



Team NO: 024
Team Name: DJS Skylark - Regular Class
School Name: Dwarkadas J. Sanghvi College of Engineering
SAE Aero Design East 2020
Size: B Scale: 1:18 Unit: inches